Hindawi
Advances in Civil Engineering
Volume 2024, Article ID 6461381, 11 pages
https://doi.org/10.1155/2024/6461381

Research Article

Real-Time Quantitative Evaluation on the Longitudinal Slip Performance of Spherical Steel Bearings of Long-Span Bridges

Shiyang Xu,[1] Xin Zhou ,[2] Gaoxin Wang,[1] and Youliang Ding[2]

[1]*State Key Laboratory for Geomechanics and Deep Underground Engineering, China University of Mining and Technology, Xuzhou, China*
[2]*The Key Laboratory of Concrete and Prestressed Concrete Structures of Ministry of Education, Southeast University, Nanjing 210096, China*

Correspondence should be addressed to Xin Zhou; zhouxin_0616@163.com

Received 25 October 2023; Revised 19 January 2024; Accepted 1 March 2024; Published 15 March 2024

Academic Editor: Pengjiao Jia

Spherical steel bearings play an important role in the normal longitudinal expansion of the main girders of long-span bridges. With the increase in service time, the wear damage will deteriorate the longitudinal slip performance of spherical steel bearings. In this research, a method of real-time quantitative evaluation on longitudinal slip performance is proposed through monitoring data analysis, correlation analysis, damage evaluation analysis, and experiment data analysis. Monitoring data analysis shows that the temperature field has a good linear relationship with longitudinal displacement. Correlation analysis shows that this relationship is well described by a time-varying multiple linear regression model. Furthermore, bearing friction is used as an index for real-time quantitative evaluation, and a large value of bearing friction indicates serious damage. An evaluation model considering the influence of temperature field and bearing frictions is proposed. The time-varying values of bearing frictions are calculated through Kalman filtering analysis. Experimental results show that the maximum evaluation error of this method is less than 5%, verifying that the proposed method is feasible for real-time quantitative evaluation on the longitudinal slip performance of bridge bearings.

1. Introduction

Spherical steel bearing is one kind of important force-bearing component for long-span bridge structures, which transfers vertical loads from superstructure to substructure and satisfies the longitudinal expansion performance of main girders as well [1–3]. A spherical steel bearing is mainly composed of a top support plate, PTFE plate (significant deformation occurring in PTFE), steel ball core, bottom support plate, and bolts. With the increase in service time, the wear damage of the PTFE plate will deteriorate the longitudinal slip performance of bearings. As shown in Figure 1, the severe wear of the PTFE plate of a suspension bridge, located in Jiangyin, increased the friction force, finally caused the PTFE plate to peel off [4]. What is more, the bearing damage always results in considerable costs and traffic interruption [5–7].

Structural temperature has a significant effect on the longitudinal displacement of bridge girders [8–15]. For example, Xia et al. [15] carried out field monitoring and numerical analysis of the temperature behavior of the Tsing Ma Suspension Bridge, and the results show that the time histories of the temperature field and its effect have very similar changing trends. Further research results show that temperature has a linear correlation with longitudinal displacement [13–15]. Using long-term monitoring data, Wang et al. [16] built the mathematical model of the linear correlation between longitudinal displacement and temperature field. The wear damage of the PTFE plate will change the linear correlation. Hence, an abnormal correlation indicates bearing damage. For example, Webb et al. [17] detected the partial damage of the flyover's pier bearings through an analysis of the correlation between pier displacement and uniform temperature.

However, the temperature field of continuous steel truss bridges is very complicated [18, 19]. There are distinct temperature differences in steel truss girders, which may have a serious impact on the longitudinal displacements of main girders [20]. In the current study, the effect of temperature

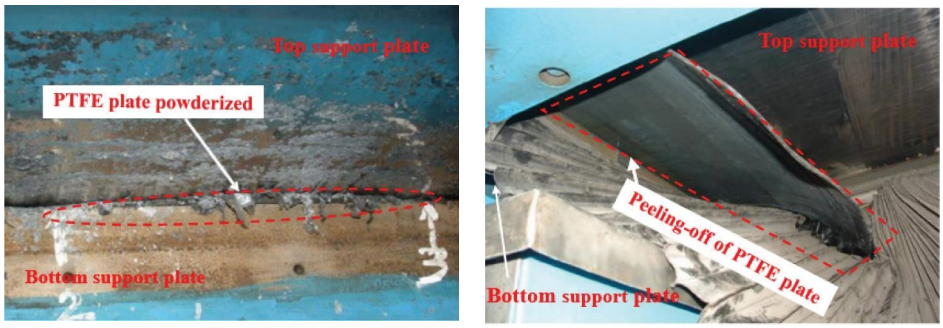

(a) (b)

Figure 1: Damage to bridge support [4]: (a) wear of PTFE plates; (b) peeling-off of PTFE plates.

differences in steel truss girders has not been thoroughly considered. In addition, continuous truss bridges usually have many bearings, and it is difficult to localize and quantify the damaged bearings in real-time. In the current study, a period of monitoring data is necessary to mathematically model the correlation between temperature and longitudinal displacement [15–17], which is not appropriate for real-time analysis.

Hence, the aim of this paper is to achieve real-time quantitative evaluation on the longitudinal slip performance of bridge bearings using the monitoring data of temperature and longitudinal displacements. In order to achieve this goal, this paper thoroughly studied the influence of complex temperature fields and bearing frictions on longitudinal displacements of bridge bearings through monitoring data analysis, correlation analysis, damage evaluation analysis, and experiment data analysis. Finally, a time-varying multiple linear regression model containing the influence of temperature field and bearing frictions is proposed for real-time quantitative evaluation on longitudinal slip performance of bridge bearings, which is verified by an experiment test.

2. Monitoring Data Analysis

2.1. Description of the Bridge and the Monitoring System. The bridge in this study is a continuous steel truss arch bridge with a total length of 1,272 m, as shown in Figure 2(a). There are seven sets of bearings, namely 1#–7#, which are movable except 4#. The upper and downstream sides of the six movable bearings are, respectively, installed with a displacement sensor, a total of 12 displacement sensors, respectively, represented by $D_{i,u}$ and $D_{i,d}$, $i = 1, 2, \ldots, 6$. All the displacement sensors are the magnetostrictive displacement sensor, the sampling frequency of which is 1 Hz. As shown in Figures 2(b) and 2(c), six temperature sensors are installed on the top chord, bottom chord, and bridge deck chord of this bridge, which are denoted by T, containing T_1–T_6. All temperature sensors are the fiber bragg grating, the sampling frequency of which is also 1 Hz.

2.2. Temperature Features. Due to the interference of the external environment of the bridge site, the monitoring data will appear abnormal phenomena, such as "spike," "jump," and "drift." As shown in Figure 3(a), the daily time–history curve of structure temperature presents distinct daily characteristics but appears at the "spike" point at about 9:45 am. In addition, from 15:30 to 20:30 pm, there are many "spikes" in the temperature curve. If the abnormal data are not processed, the accuracy of the analysis will be affected. The time window smoothing method is mostly used to solve this problem [21, 22]. The length of the time window is depended on the data scale and timeliness, which is 10 min in this paper, i.e., the raw data will be averaged every 10 min. The daily time–history curve of T becomes smooth after 10-min averaged in Figure 3(a). The structure temperature data after processing is named TP, containing TP_1–TP_6, which is used for correlation analysis and correlation model construction below. The daily time-history of structure temperature on the 13th day is shown in Figure 3(b); we can see that the daily time–history curves are similar to a sine wave, and there is a temperature gradient (TG) in the main beam.

Temperature is mainly affected by solar radiation. T_1 and T_2 are located on the top chord, which is significantly affected by sunlight, while T_5 and T_6 are located on the bottom plate of the bridge, which are not exposed to sunlight. Therefore, the TG is investigated, which is denoted by TP_{ij} (namely, $TP_{ij} = TP_i - TP_j$). TG contains TG between two sides of a single chord (TGS) and TG between different chord members (TGM) in this paper. The average values are used to represent the uniform temperature TP_u (namely, $TP_u = (TP_1 + TP_2)/2$), TP_m (namely, $TP_m = (TP_3 + TP_4)/2$), and TP_d (namely, $TP_d = (TP_5 + TP_6)/2$). The maximum and minimum values of temperature differences are shown in Table 1. It can be seen that there are significant TGs in this bridge; the maximum and minimum of TGS are 5.76 and −11.81°C, respectively. The maximum and minimum of TGM are 11.16 and −7.66°C, respectively. Hence, both TGS and TGM should be taken into consideration in the analysis of the temperature effect on the longitudinal displacement.

2.3. Displacement Features. The longitudinal displacement of each set of bearings is measured by two displacement sensors; the average value of two measured displacements is calculated to represent the displacement of each set of bearings in this paper, which are denoted as D_1–D_6. In the raw data, the longitudinal displacement is caused by many factors, such as vehicle, train, wind loads, etc. Figure 4 shows the

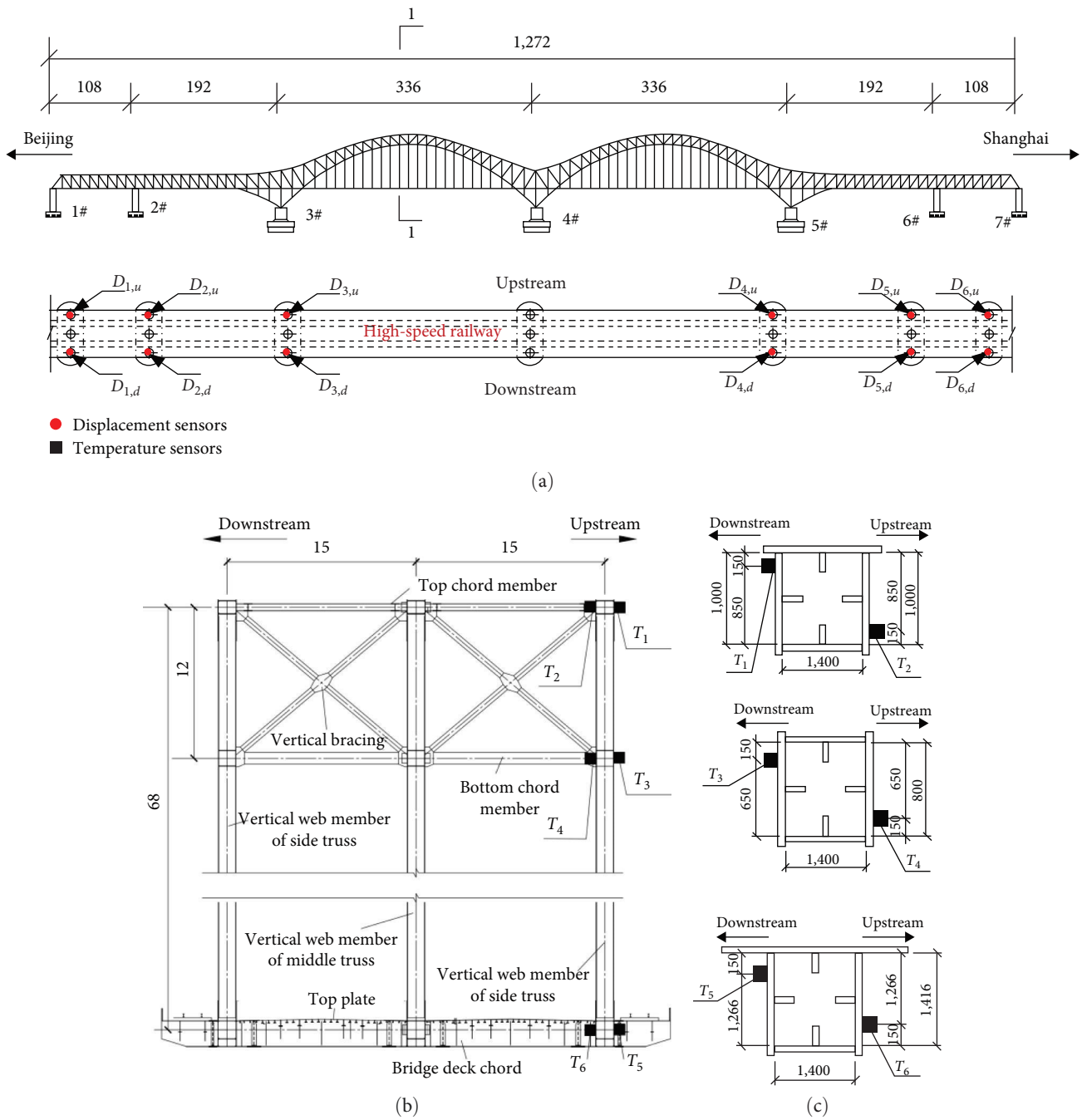

Figure 2: Deployment of sensors of the continuous steel truss arch bridge: (a) elevation of the bridge and displacement sensors (unit: m); (b) Section 1-1 (unit: m); (c) chord member section (unit: mm).

extraction process of temperature-induced displacement (TID). Wavelet decomposition is usually used for filtering the raw data to get the TID, which is the low-frequency information [23]. Then, the displacements after filtering are averaged every ten minutes to get the same length of temperature data; the displacement data after processing is named DP, containing DP_1–DP_6, which is used for correlation analysis and correlation model construction below.

The time–history curve of TP_1, TP_3, and DP_1 is shown in Figure 5; it can be seen that the time–history curve of TP_1, TP_3, and DP_1 has very similar changing trends and presents distinct seasonal characteristics during the sampling period. In addition, according to the previous analysis, there is significant TG in these steel truss bridges, which should be taken into consideration.

3. Correlation Modeling Analysis

In this paper, the correlation coefficient R, shown in Equation (1), is introduced to describe the correlation between TP and DP, which is between 0 and 1, and the larger R is, the stronger the correlation between variables.

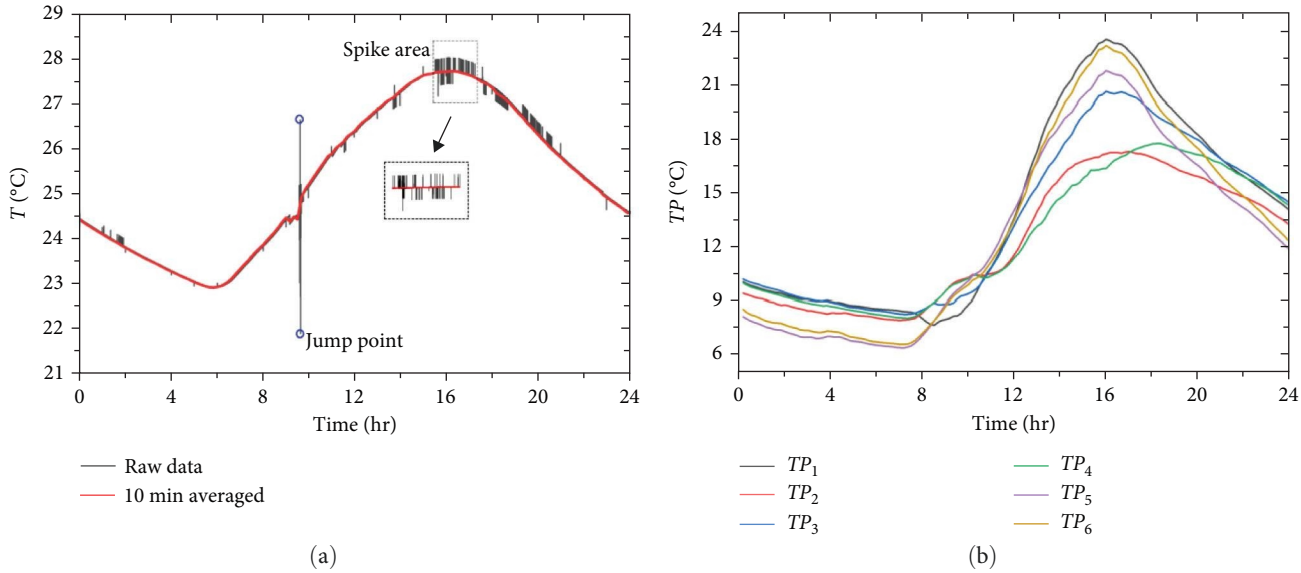

Figure 3: Temperature data processing and daily time–history curve of temperature sensors: (a) temperature data processing; (b) temperature time–history on the 13th day.

Table 1: Temperature difference threshold during the sampling period.

Temperature type	Temperature difference	Maximum value (°C)	Minimum value (°C)
TGS	$TP_{1,2}$	3.60	−4.10
	$TP_{3,4}$	5.17	−11.81
	$TP_{5,6}$	5.76	−11.16
TGM	$TP_{u,m}$	4.10	−3.60
	$TP_{m,d}$	11.16	−5.76
	$TP_{u,d}$	9.32	−7.66

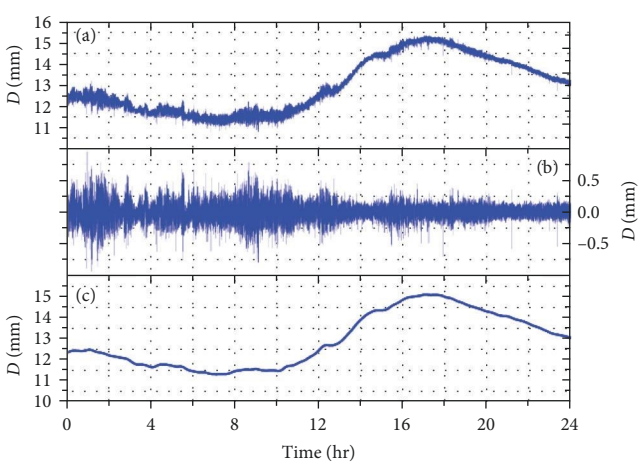

Figure 4: Temperature-induced displacement extraction: (a) raw data; (b) high-frequency displacement; (c) temperature-induced displacement.

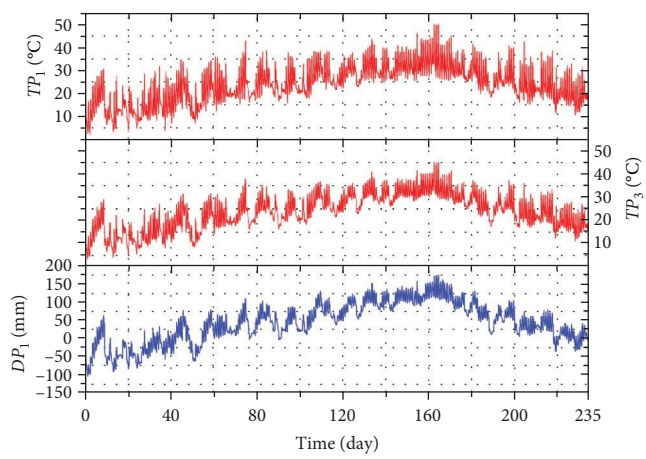

Figure 5: Time–history curve of TP_1, TP_3, and DP_1 during the sampling period.

$$R_{n,m} = \frac{\sum_{i=1}^{N}\left(DP_{n,i} - \overline{DP_n}\right)\left(TP_{m,i} - \overline{TP_m}\right)}{\sqrt{\sum_{i=1}^{N}\left(DP_{n,i} - \overline{DP_n}\right)^2}\sqrt{\sum_{i=1}^{N}\left(TP_{m,i} - \overline{TP_m}\right)^2}}, \quad (1)$$

where $R_{n,m}$ denotes the correlation coefficient between DP_n and TP_m, $DP_{n,i}$ denotes the ith value of DP_n, $TP_{m,i}$ denotes the ith value of TP_m, $\overline{DP_n}$ and $\overline{TP_n}$ denotes the average value of DP_n and TP_m, respectively, N denotes the total amount of data. In this paper, $n = 1, 2, \ldots 6$ and $m = 1, 2, \ldots, 6$.

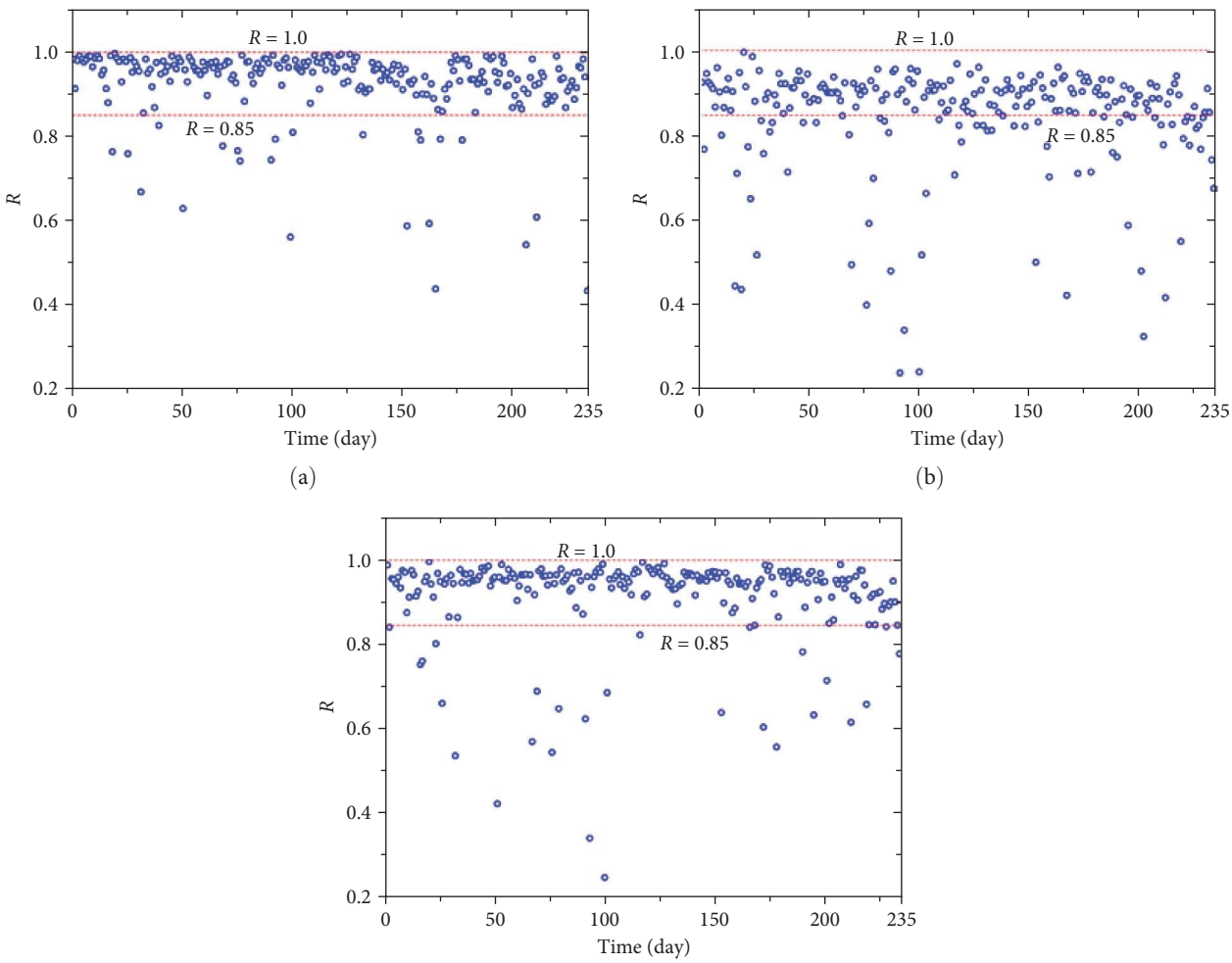

Figure 6: Scatter diagram of correlation coefficient: (a) $R_{1,1}$ (DP_1 and TP_1); (b) $R_{1,3}$ (DP_1 and TP_3); (c) $R_{1,5}$ (DP_1 and TP_5).

According to Equation (1), the daily correlation coefficient between DP and TP can be calculated. Figure 6 is the scatter diagram of the daily correlation coefficient of TP_1, TP_3, TP_5 versus DP_1; we can see that there is a significant positive correlation between the TID and temperature, and the correlation coefficient R is mainly 0.85–1.0. Hence, a linear regression model is appropriately used to describe this linear correlation. To consider the temperature variables between chords, TP_1–TP_6 are used temperature variables in this linear regression model.

The model is a multiple regression equation as follows:

$$DP_j(t) = \gamma_{1,j}TP_1(t) + \gamma_{2,j}TP_2(t) + \ldots + \gamma_{N,j}TP_N(t) + C_j, \tag{2}$$

where $DP_j(t)$ denotes the regression value of the DP_j at time t, $j = 1, 2, \ldots, M$. $TP_i(t)$ denotes TP_i at time t, $i = 1, 2, \ldots, N$. $\gamma_{i,j}$ denotes the linear constant coefficient between $TP_i(t)$ and $DP_j(t)$, and C_j is the constant term. In this paper, $M = 6$ and $N = 6$.

In Equation (2), a long period of monitoring temperature and displacement data is needed to determine the values of $\gamma_{i,j}$, so Equation (2) is not suitable for real-time analysis. Real-time analysis helps to identify the bearing damage in time, so Equation (2) is modified into a time-varying linear regression equation as follows:

$$\begin{aligned} DP_j(t) = {} & \gamma_{1,j}(t)TP_1(t) + \gamma_{2,j}(t)TP_2(t) \\ & + \ldots + \gamma_{N,j}(t)TP_N(t) + C_j, \end{aligned} \tag{3}$$

where $\gamma_{i,j}(t)$ denotes the time-varying linear regression coefficient of at time t.

However, the time histories of TP_1–TP_6 have similar changing trends, which are not suitable to be treated as independent variables. Principal components analysis is used to extract the principal components of the temperature field, which are independent. The principal components of temperature are sorted according to the contribution rate, and the greater the contribution rate, the more original information contained in the principal component. As shown in Figure 7(a), the six temperature principal components,

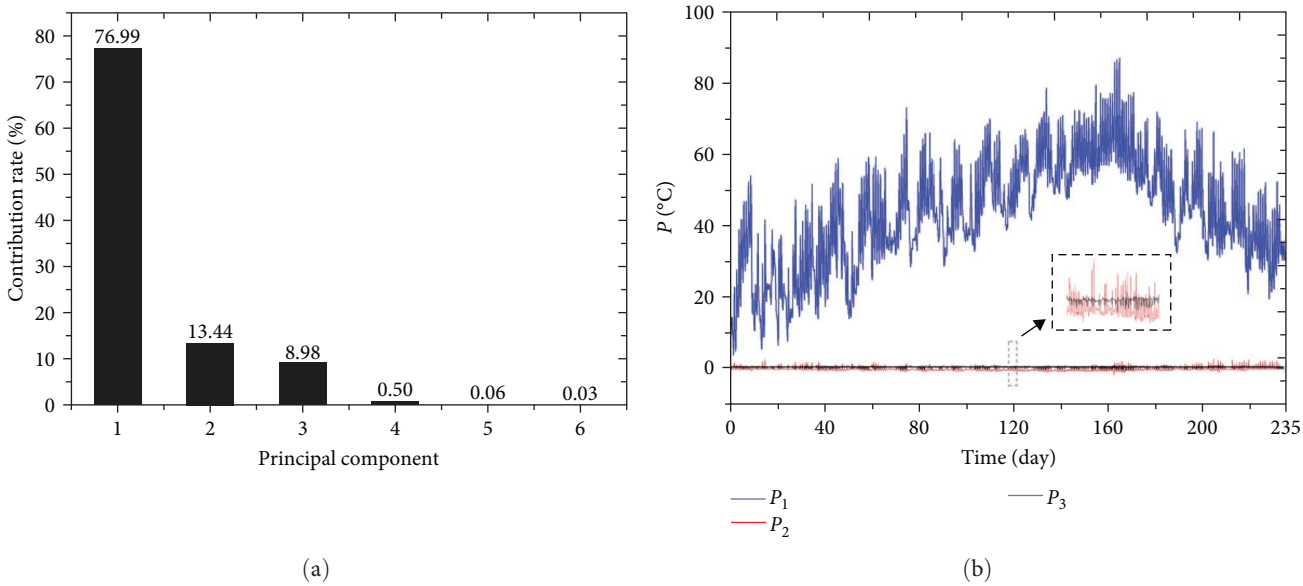

Figure 7: Temperature principal component: (a) principal component contribution rate; (b) time–history curve of P_1, P_2, P_3.

denoted as P_1–P_6, are ranked in descending order of contribution rate. We can see that the cumulative contribution rate of P_1, P_2, and P_3 is 99.41%, and the trends of the time–history curves of them are different, as shown in Figure 7(b). The principal components are independent of each other, which can be treated as independent variables. Hence, Equation (3) is changed as follows:

$$DP_j(t) = \gamma_{1,j}(t)P_1(t) + \gamma_{2,j}(t)P_2(t) + \ldots + \gamma_{Q,j}(t)P_Q(t) + C_j. \tag{4}$$

Kalman filtering method is used to determine the values of $\gamma_{i,\ j}(t)$. In this method, a state equation is given as follows:

$$\Psi_j(t) = \Omega_j \Psi_j(t-1) + V_j(t), \tag{5}$$

where $\Psi_j(t)$ is a column vector of containing time-varying parameters $\gamma_{i,\ j}(t)$, i.e.,$\Psi_j(t) = (\gamma_{1,j}(t)\ \gamma_{2,j}(t)\ \ldots\ \gamma_{Q,\ j}(t)]^T$. Ω_j is an iteration matrix. $V_j(t)$ is a column vector of containing white noises. By virtual of Equations (4) and (5), the values of $\gamma_{i,\ j}(t)$ are determined using the Kalman filtering method. For example, the values of P_1, P_2, P_3, and DP_1 of the bridge are substituted into Equation (4), and then the values of $\gamma_{1,1}(t)$, $\gamma_{1,2}(t)$, and $\gamma_{1,3}(t)$ are determined, as shown in Figure 8(a). It can be seen that the changing trends of $\gamma_{1,1}(t)$, $\gamma_{1,2}(t)$, and $\gamma_{1,3}(t)$ are stationary with time after a quick convergence. The changing trends help to identify the bearing damage. If the bearing is in good health, the time-varying coefficient tends to be flat; otherwise, the damage is occurring. Hence, Figure 8(a) indicates that the bearing 1# is in good health during the monitoring period. The result is correct because the model is established based on the data of the bridge in the early stage of operation.

In order to verify the accuracy of Equation (4), the $P_1(t)$, $P_2(t)$, $P_3(t)$, $\gamma_{1,1}(t)$, $\gamma_{1,2}(t)$, and $\gamma_{1,3}(t)$ are substituted into Equation (4) to obtain the simulated $DP_{1,s}(t)$. Then, the simulated and monitoring displacements are compared, as shown in Figure 8(b). It can be seen that the simulated values are very close to the monitoring values, indicating that it is appropriate to use Equation (4) for a description of the correlation. Figures 8(c) and 8(d) show the time-history curves of calculated and measured values at the early and late sampling periods, respectively; we can see that as the amount of data increases, the simulated values become more accurate.

4. Damage Evaluation Analysis

As mentioned above, the temperature field of bridge girders has an effect on bearing displacements. The wear damage inside the bearings will cause friction, existing between the steel ball core and the PTFE plate, which prevents the bearings from moving, as illustrated in Figure 9. Therefore, when bearing wear occurs, the longitudinal displacement is also affected by the friction, which is modeled by an equation as follows:

$$DP_j(t) = DP_{j,T}(t) - DP_{j,f}(t), \tag{6}$$

where $DP_j(t)$ denotes the total displacement of the jth bearing at time t. $DP_{T,j}(t)$ denotes the displacement caused by structure temperature at time t, and $DP_{f,j}(t)$ denotes the displacement caused by friction at time t. $DP_{j,\ T}(t)$ has a good linear correlation with structure temperature, which is expressed as Equation (7a), and $DP_{j,\ f}(t)$ is expressed as Equation (7b).

$$\begin{aligned} DP_{j,T}(t) = {} & \gamma_{1,j}(t)P_1(t) + \gamma_{2,j}(t)P_2(t) \\ & + \ldots + \gamma_{Q,j}(t)P_Q(t) + C_j, \end{aligned} \tag{7a}$$

$$\begin{aligned} DP_{j,f}(t) = {} & \sum_{k=1}^{M} f_k(t)\delta_1 + \sum_{k=2}^{M} f_k(t)\delta_2 + \ldots \\ & + \sum_{k=j}^{M} f_k(t)\delta_j,\ 1 \le k, j \le M, \end{aligned} \tag{7b}$$

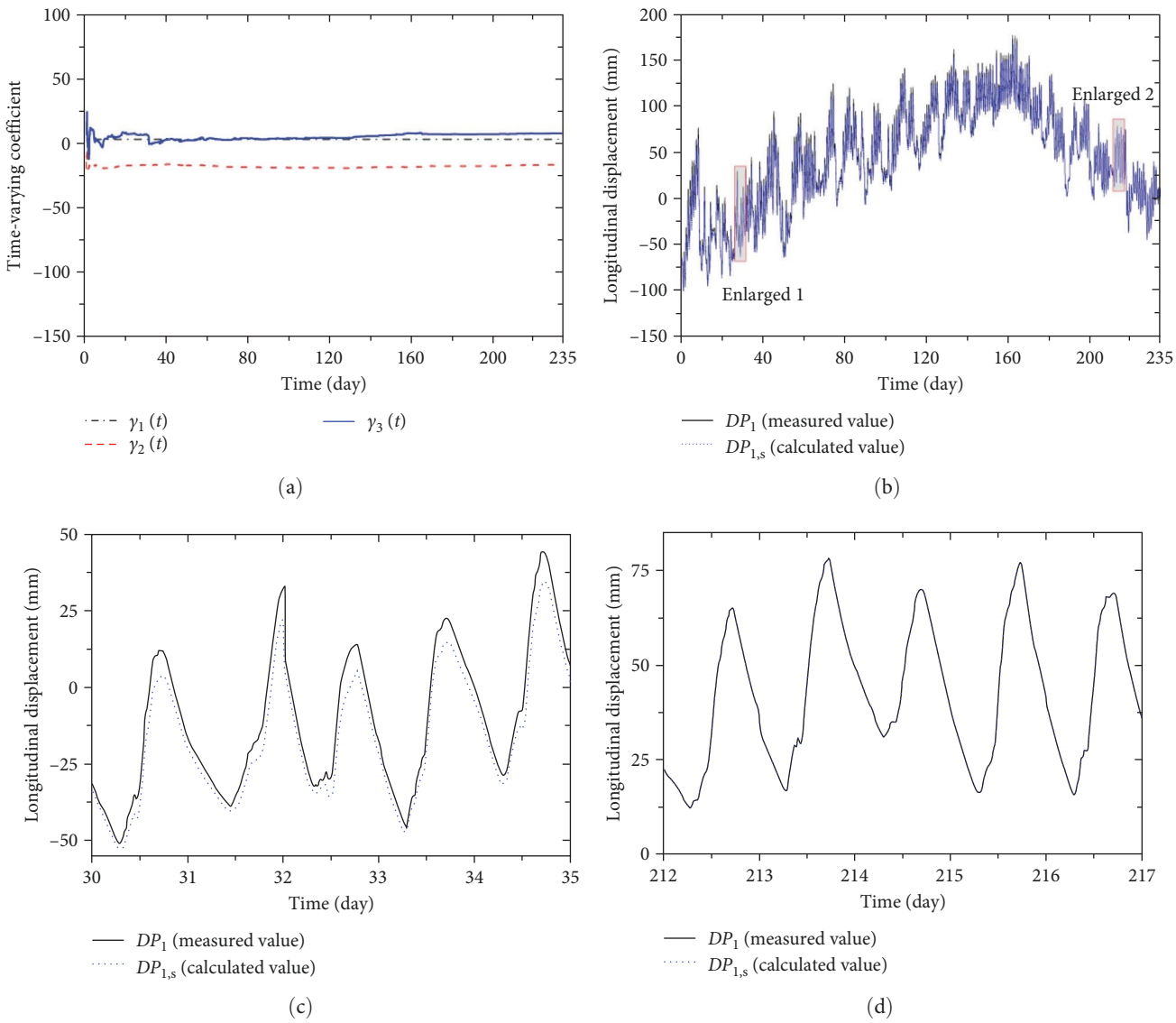

Figure 8: Time varying coefficient and the calculated and measured values of Bearing 1#: (a) time-varying coefficient; (b) calculated value and measured value; (c) Enlarged 1; (d) Enlarged 2.

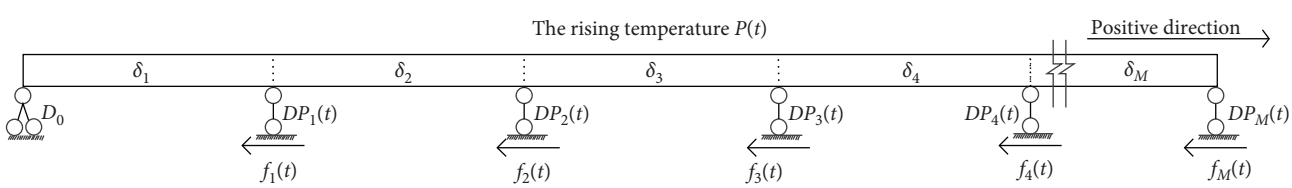

Figure 9: Illustration of bearing displacements caused by temperature field and frictions.

where $f_j(t)$ denotes the friction of the jth bearing, δ_j denotes the jth longitudinal flexibility coefficient.

When the sliding friction of the bridge bearings increases, it indicates that the sliding plates inside the bearings are worn. Therefore, the wear condition of bearings can be evaluated in real time by monitoring the change of bearing friction force in real time. The specific calculation method of bearing friction is described as follows:

(1) The temperature field and displacement monitoring data are substituted into Equations (6) and (7), so the displacement residual $R_j(t)$ includes the friction force of the bearings as follows:

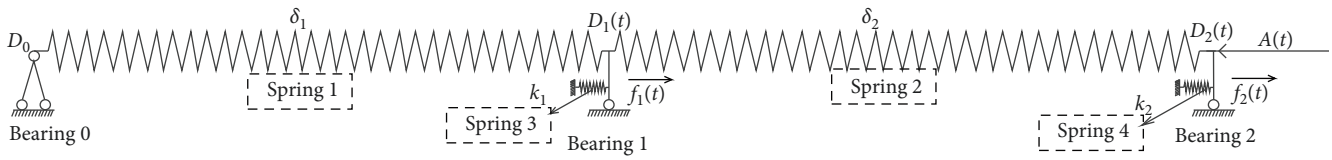

Figure 10: The drawing of the experiment model.

$$\begin{bmatrix} R_1(t) \\ R_2(t) \\ \vdots \\ R_M(t) \end{bmatrix} = \begin{bmatrix} DP_1(t) \\ DP_2(t) \\ \vdots \\ DP_M(t) \end{bmatrix} - \begin{bmatrix} DP_{1,\mathrm{T}}(t) \\ DP_{2,\mathrm{T}}(t) \\ \vdots \\ DP_{M,T}(t) \end{bmatrix} = \begin{bmatrix} D_{1,\mathrm{f}}(t) \\ D_{2,\mathrm{f}}(t) \\ \vdots \\ D_{M,f}(t) \end{bmatrix} + \begin{bmatrix} e_1(t) \\ e_2(t) \\ \vdots \\ e_M(t) \end{bmatrix}, \tag{8}$$

where $e_j(t)$ is a stationary sequence with a mean value of zero caused by model fitting error. Combined Equation (6), $R_j(t)$ ($j = 1, 2, \cdots, M$) can be furthermore represent as follows:

$$\begin{bmatrix} R_1(t) \\ R_2(t) \\ \vdots \\ R_M(t) \end{bmatrix} = \begin{bmatrix} \sum_{k=1}^{M} f_{\mathrm{k}}(t)\delta_1 \\ \sum_{k=1}^{M} f_{\mathrm{k}}(t)\delta_1 + \sum_{k=2}^{M} f_{\mathrm{k}}(t)\delta_2 \\ \vdots \\ \sum_{k=1}^{M} f_{\mathrm{k}}(t)\delta_1 + \sum_{k=2}^{M} f_{\mathrm{k}}(t)\delta_2 + \ldots + f_M(t)\delta_M \end{bmatrix} + \begin{bmatrix} e_1(t) \\ e_2(t) \\ \vdots \\ e_M(t) \end{bmatrix}. \tag{9}$$

(2) $R_j(t) - R_{j-1}(t)$ represented by $\Delta R_{jj-1}(t)$, is calculated to reduce repetitive frictional terms as follows:

$$\begin{bmatrix} \Delta R_{10}(t) \\ \Delta R_{21}(t) \\ \vdots \\ \Delta R_{MM-1}(t) \end{bmatrix} = \begin{bmatrix} \sum_{k=1}^{M} f_{\mathrm{k}}(t)\delta_1 \\ \sum_{k=2}^{M} f_{\mathrm{k}}(t)\delta_2 \\ \vdots \\ f_M(t)\delta_M \end{bmatrix} + \begin{bmatrix} \vartheta_{10}(t) \\ \vartheta_{21}(t) \\ \vdots \\ \vartheta_{MM-1}(t) \end{bmatrix} = \begin{bmatrix} \delta_1 & \delta_1 & \ldots & \delta_1 \\ 0 & \delta_2 & \ldots & \delta_2 \\ 0 & 0 & \ddots & \vdots \\ 0 & 0 & 0 & \delta_M \end{bmatrix}_{M\times M} \begin{bmatrix} f_1(t) \\ f_2(t) \\ \vdots \\ f_M(t) \end{bmatrix} + \begin{bmatrix} \vartheta_{10}(t) \\ \vartheta_{21}(t) \\ \vdots \\ \vartheta_{MM-1}(t) \end{bmatrix}, \tag{10}$$

where $\vartheta_{jj-1}(t)$ is the difference of model fitting error $e_j(t)$ ($\vartheta_{jj-1}(t) = e_j(t)\text{-}e_{j-1}(t)$).

(3) The friction force of each bearing can be calculated by transforming Equation (10) as follows:

$$\begin{bmatrix} f_1(t) \\ f_2(t) \\ \vdots \\ f_M(t) \end{bmatrix} = \begin{bmatrix} \Delta_1 & \delta_1 & \ldots & \delta_1 \\ 0 & \Delta_2 & \ldots & \Delta_2 \\ 0 & 0 & \ddots & \vdots \\ 0 & 0 & 0 & \delta_M \end{bmatrix}_{M\times M}^{-1} \begin{bmatrix} \Delta R_{10}(t) - \vartheta_{10}(t) \\ \Delta R_{21}(t) - \vartheta_{21}(t) \\ \vdots \\ \Delta R_{MM-1}(t) - \vartheta_{MM-1}(t) \end{bmatrix}. \tag{11}$$

Then the vector set of $f_j(t)$ is denoted by $F(t)$, the vector set of δ_j is denoted by Φ, and the vector set of $\Delta R_{jj-1}(t) - \vartheta_{jj-1}(t)$ is denoted byω. Equation (11) is simplified as follows:

$$F(t) = \phi^{-1}\omega. \tag{12}$$

The daily maximum values of $F(t)$ are selected, denoted by $F_v(t)$, during the sampling period ($F_v(t) = (f_{1,v}(t)\, f_{2,v}(t) \ldots f_{M,v}(t))^T$). Then, the fitting curves of $F_v(t)$, represented by $M_j(t)$, can be obtained based on $F_v(t)$. Finally, the degraded bearings can be identified and evaluated according to the trend of $M_j(t)$. For example, when $M_j(t)$ shows an increasing trend, it means that bearing j is in a degraded state. Otherwise, bearing j is healthy.

5. Experiment Test Analysis

5.1. Description of Experiment Design. The experiment model is a two-span continuous beam bridge with three bearings, as shown in Figure 10. Bearing 1# is fixed on the test bench, and Bearings 2# and 3# are movable in the longitudinal direction, which are simulated by pulleys. The bridge girder is simulated by Springs 1 and 2 ($\delta_1 = 4.17$ mm/N, $\delta_2 = 2.63$ mm/N). The friction forces of bearings are simulated by Springs 3 and 4, i.e., the compression of each spring produces a force $f_1(t)$ or $f_2(t)$ that prevents the bearing from moving. Because it is difficult to simulate temperature action $P_{\mathrm{i}}(t)$, an actuator is used to apply a horizontal load $A(t)$ on the one end of the girder to simulate the influence of $P_{\mathrm{i}}(t)$ on displacement. This is feasible because $A(t)$ also has a linear correlation with $D(t)$. $A(t)$ is measured by a high-precision pressure sensor, which is located between the beam end and the actuator. Red marks

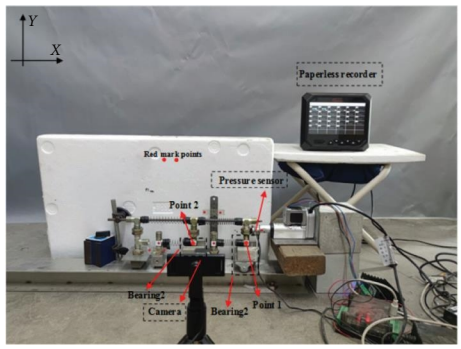

Figure 11: The experiment test.

Table 2: Experiment data.

t	$D_1(t)$ (mm)	$D_2(t)$ (mm)	$A(t)$ (N)	$f(t)$ (N)				E_1	E_2
				$f_{1,\ m}(t)$	$f_{2,\ m}(t)$	$f_{1,\ a}(t)$	$f_{2,\ m}(t)$		
1	0.96	2.17	0.95	0.23	0.49	0.22	0.47	4.53	4.66
2	1.93	4.33	1.89	0.45	0.98	0.45	0.94	1.49	4.03
3	2.86	6.45	2.8	0.68	1.43	0.66	1.4	2.66	2.42
4	3.82	8.59	3.66	0.9	1.85	0.88	1.86	1.66	0.97
5	4.79	10.74	4.57	1.11	2.31	1.11	2.33	0.63	0.99
6	5.75	12.86	5.43	1.32	2.73	1.33	2.79	0.73	2.22
7	6.71	14.99	6.27	1.54	3.13	1.55	3.25	0.86	3.84
8	7.66	17.14	7.23	1.76	3.63	1.77	3.72	0.55	2.46
9	8.6	19.24	8.09	1.98	4.05	1.99	4.18	0.44	3.12
10	9.59	21.48	9.06	2.22	4.54	2.22	4.66	0.03	2.65
11	10.58	23.71	9.96	2.45	4.97	2.45	5.15	0.2	3.33
12	11.57	25.84	10.84	2.65	5.42	2.67	5.61	1.04	3.37
13	12.53	27.95	11.7	2.86	5.84	2.89	6.07	1.26	3.76
14	13.48	30.06	12.58	3.07	6.28	3.11	6.52	1.52	3.71

are pasted at the bottom of the bearings, as shown in Figure 11. When the bearings move, a camera will track the displacements $D_i(t)$ of the centroids of red mark points using the image recognition algorithm [24]. Under this experiment condition, Equations (11) and (12) are written as follows:

$$F(t) = \begin{bmatrix} f_1(t) \\ f_2(t) \end{bmatrix} = \Phi^{-1}\omega, \tag{13a}$$

$$\Phi = \begin{bmatrix} 4.17 & 4.17 \\ 0 & 2.63 \end{bmatrix}, \tag{13b}$$

$$\omega = \begin{bmatrix} \gamma_1 A(t) - D_1(t) + C_1 \\ (\gamma_1 - \gamma_2)A(t) - [D_2(t) - D_1(t)] + C_2 - C_1 \end{bmatrix}. \tag{13c}$$

5.2. Experimental Result. In this experiment, $A(t)$ is loaded in 14 steps produced by an actuator, and the values of $D_1(t)$ and $D_2(t)$ are measured by the camera. The values in each step are shown in Table 2. Then, by substituting $A(t)$, $D_1(t)$, and $D_2(t)$ into Equations (6) and (7), the values of $f_1(t)$ and $f_2(t)$ are determined using the proposed method, as shown in Table 2. In addition, the actual friction values $f_{1a}(t)$ and $f_{1a}(t)$ of Bearings 1 and 2 are calculated according to Hooke's law by Equation (14a), as shown in Table 2. The relative errors E_1 and E_2 are calculated by Equation (14b), as shown in Table 1.

$$f_{ia}(t) = k_i D_i(t), \tag{14a}$$

$$E_i = \frac{|f_i(t) - f_{ia}(t)|}{f_{ia}(t)} 100\%, \tag{14b}$$

where k_i is the stiffness coefficient of the Spring 3 or 4 ($k_1 = 0.24$N/mm, $k_2 = 0.38$N/mm), $i = 1,2$. It can be seen from Table 2 that $f_i(t)$ is close to $f_{ia}(t)$, and the relative error is less than 5%, verifying that the proposed method is feasible for real-time quantitative evaluation on bearing damage of continuous beam bridges.

6. Conclusion

In this research, a method of real-time quantitative evaluation on the longitudinal slip performance of spherical steel bearings is proposed through monitoring data analysis, correlation modeling analysis, damage evaluation analysis, and experiment test analysis. The main conclusions are drawn as follows:

(1) The longitudinal displacement of the bearing exhibits a strong linear correlation with the monitored temperature. Since temperature and displacement change at every moment, a constant coefficient model cannot dynamically describe the real-time the longitudinal slip performance of the bearings. Then, a multiple linear regression model with time-varying coefficients is proposed, and the time-varying coefficients in the model are solved by the Kalman filter method. This model describes the longitudinal displacement of the bearing accurately and can help to identify bearing damage.

(2) Considering the influence of temperature field and bearing frictions, a time-varying multiple linear regression model is proposed for real-time quantitative evaluation of the longitudinal slip performance of spherical steel bearings. In this model, time-varying bearing friction is used as an evaluation index, which is used for real-time quantitative evaluation. Experimental analysis shows that the maximum evaluation error is less than 5%, verifying that the proposed method is feasible for real-time quantitative evaluation.

(3) There are significant vertical and transversal temperature differences between truss members in steel truss bridges. A suggestion is that significant vertical and transversal temperature differences should be taken into consideration in the analysis of temperature effects.

Data Availability

Data are available on request from the authors.

Conflicts of Interest

The authors declare that they have no conflicts of interest.

Acknowledgments

The authors gratefully acknowledge the National Natural Science Foundation of China (grant number 51908545) and the 2021 Science and Technology R&D Project (Science and Technology Project of State Grid Jiangsu Electric Power Co., Ltd.) (no. J2021022). This work was supported by the Innovative and Entrepreneurial Talent Plan of Jiangsu Province of China and the Natural Science Foundation of Jiangsu Province of China (grant number BK20180652).

References

[1] J. W. Zhan, H. Xia, and N. Zhang, "A diagnosis method for bridge rubber support disease based on impact responses," *Journal of Vibration & Shock*, vol. 32, no. 8, pp. 153–140, 2013.

[2] T. H. Yi, H. N. Li, and M. Gu, "Recent research and applications of GPS based technology for bridge health monitoring," *Science China Technological Sciences*, vol. 53, no. 10, pp. 2597–2610, 2010.

[3] N. D. Battista, R. Westgate, and K. Y. Koo, "Wireless monitoring of the longitudinal displacement of the Tamar suspension bridge deck under changing environmental conditions," *International Society for Optics and Photonics*, 2011.

[4] T. Guo, J. Liu, and L. Huang, "Investigation and control of excessive cumulative girder movements of long-span steel suspension bridges," *Engineering Structures*, vol. 125, pp. 217–226, 2016.

[5] X. Yan, H. Xie, and T. Wang, "A multiple linear regression data predicting method using correlation analysis for wireless sensor networks," *Journal of Computer Information Systems*, vol. 7, no. 11, pp. 4105–4112, 2011.

[6] Z. B. Lan and M. N. Li, "Handling of bearing disengagement from a curved steel box girder with heavy longitudinal slope and sharp radius," *Bridge Construction*, 2014.

[7] Z. Feng, J. Huo, H. Hu et al., "Research on corrosion damage and bearing characteristics of bridge pile foundation concrete under a dry–wet–freeze–thaw cycle," *Advances in Civil Engineering*, vol. 2021, no. 6, Article ID 8884396, 13 pages, 2021.

[8] D. Wang, Y. Liu, and Y. Liu, "3D temperature gradient effect on a steel–concrete composite deck in a suspension bridge with field monitoring data," *Structural Control and Health Monitoring*, vol. 25, no. 7, Article ID e2179, 2018.

[9] W. Gaoxin and D. Youliang, "Research on monitoring temperature difference from cross sections of steel truss arch girder of Dashengguan Yangtze bridge," *International Journal of Steel Structures*, vol. 15, no. 3, pp. 647–660, 2015.

[10] G.-X. Wang, Y.-L. Ding, P. Sun, L.-L. Wu, and Q. Yue, "Assessing static performance of the Dashengguan Yangtze bridge by monitoring the correlation between temperature field and its static strains," *Mathematical Problems in Engineering*, vol. 2015, Article ID 946907, 12 pages, 2015.

[11] S. R. Abid, F. Mussa, N. Taysi, and M. Özakça, "Experimental and finite element investigation of temperature distributions in concrete-encased steel girders," *Structural Control and Health Monitoring*, vol. 25, no. 1, Article ID e2042, 2018.

[12] Y. Liu, Z. Qian, and H. Hu, "Thermal field characteristic analysis of steel bridge deck during high-temperature asphalt pavement paving," *KSCE Journal of Civil Engineering*, vol. 20, no. 7, pp. 2811–2821, 2016.

[13] G. Peng, S. Nakamura, and X. Zhu, "An experimental and numerical study on temperature gradient and thermal stress of CFST truss girders under solar radiation," *Computers & Concrete*, vol. 20, no. 5, pp. 605–616, 2017.

[14] J. Liu, Y. Liu, L. Jiang, and N. Zhang, "Long-term field test of temperature gradients on the composite girder of a long-span cable-stayed bridge," *Advances in Structural Engineering*, vol. 22, no. 13, pp. 2785–2798, 2019.

[15] Y. Xia, B. Chen, X.-Q. Zhou, and Y.-L. Xu, "Field monitoring and numerical analysis of Tsing Ma Suspension Bridge temperature behavior," *Structural Control and Health Monitoring*, vol. 20, no. 4, pp. 560–575, 2013.

[16] G. X. Wang, Y. L. Ding, and Y. S. Song, "Detection and location of the degraded bearings based on monitoring the longitudinal expansion performance of the main girder of the Dashengguan Yangtze bridge," *Journal of Performance of Constructed Facilities*, Article ID 04015074, 2016.

[17] G. T. Webb, P. J. Vardanega, P. R. A. Fidler, and C. R. Middleton, "Analysis of structural health monitoring

data from hammersmith flyover," *Journal of Bridge Engineering*, vol. 19, no. 6, Article ID 05014003, 2014.

[18] Y. L. Ding and G. X. Wang, "Evaluation of dynamic load factors for a high-speed railway truss arch bridge," *Shock and Vibration*, vol. 2016, Article ID 5310769, 15 pages, 2016.

[19] L. Zhou, Y. Xia, J. M. W. Brownjohn, and K. Y. Koo, "Temperature analysis of a long-span suspension bridge based on field monitoring and numerical simulation," *Journal of Bridge Engineering*, vol. 21, no. 1, Article ID 04015027, 2016.

[20] G.-X. Wang, Y.-L. Ding, X.-J. Wang, X. Yan, and Y.-F. Zhang, "Long-term temperature monitoring and statistical analysis on the flat steel-box girder of Sutong Bridge," *Journal of Highway and Transportation Research and Development*, vol. 8, no. 4, pp. 63–68, 2014.

[21] Y. Zhou, L. Sun, Z. Fu, Z. Jiang, and P. Ren, "General formulas for estimating temperature-induced mid-span vertical displacement of cable-stayed bridges," *Engineering Structures*, vol. 221, Article ID 111012, 2020.

[22] Y. Zhou and L. Sun, "Insights into temperature effects on structural deformation of a cable-stayed bridge based on structural health monitoring," *Structural Health Monitoring*, vol. 18, no. 3, pp. 778–791, 2019.

[23] T. Guo, J. Liu, Y. Zhang, and S. Pan, "Displacement monitoring and analysis of expansion joints of long-span steel bridges with viscous dampers," *Journal of Bridge Engineering*, vol. 20, no. 9, Article ID 04014099, 2015.

[24] T. Khuc and F. N. Catbas, "Computer vision-based displacement and vibration monitoring without using physical target on structures," *Structure & Infrastructure Engineering*, pp. 505–516, 2016.